Journal of Materials and Environmental Science
ISSN : 2028-2508
e-ISSN : 2737-890X
CODEN : JMESCN

J. Mater. Environ. Sci., 2025, Volume 16, Issue 11, Page 2140-2161

http://www.jmaterenvironsci.com

Two-year Comparative Study of the Corrosion Inhibition Efficiency of *Glycyrrhiza uralensis* Extracts for D16T Aluminum Alloy in Alkaline Medium

Talapova A. P., Uzakbay G. B., Akatyev N. V. *

Faculty of Natural and Geographical sciences M. Utemisov West Kazakhstan University, 090000, Uralsk, Kazakhstan

**Corresponding author, Email address: n.akatyev.science@gmail.com*

Received *01 Oct 2025,*
Revised *25 Oct 2025,*
Accepted *26 Oct 2025*

Keywords:
- ✓ *Glycyrrhiza uralensis;*
- ✓ *Aluminum alloy;*
- ✓ *Green inhibitors;*
- ✓ *Plant extracts;*
- ✓ *Metal protection*

Citation*: Talapova A.P., Uzakbay G.B., Akatyev N.V. (2025) Two-year Comparative Study of the Corrosion Inhibition Efficiency of Glycyrrhiza uralensis Extracts for D16T Aluminum Alloy in Alkaline Medium, J. Mater. Environ. Sci., 16(11), 2140-2161*

Abstract: In this work, the inhibitory properties of aqueous extracts of Ural licorice (*Glycyrrhiza uralensis*) for aluminum alloy D16T in 0.1 mol·dm^{-3} NaOH solution were studied. The kinetic, thermodynamic, and activation parameters of the corrosion process were determined. Using gravimetric and electrochemical methods, it was found that extracts obtained from the leaves demonstrate the best protective effectiveness, reaching 88.38% at maximum inhibitor concentration and increased temperature. It was shown that the formation of a protective layer on the metal surface occurs as a process of spontaneous physisorption ($\Delta G^0_{ads} > 20$ kJ·mol^{-1}) obeys the Langmuir, Freundlich, and Frumkin adsorption models, indicating the complexity of the adsorption process. It was also found that the plant samples collected in 2024 demonstrate a higher degree of corrosion protection than the samples collected in the same place of growth in 2023, and their adsorption on the D16T aluminum alloy surface obeys the same adsorption models. It is assumed that such changes are the result of the heavy spring flood of 2024. Water stress led to the rise of the synthesis of the same types of biologically active phytocomponents responsible for the adsorption on metal surface and, thereby, to the increase in anticorrosive activity.

1. Introduction

Aluminum corrosion is a universal process that significantly affects both industry and the environment. Industrially, it is generally considered beneficial because the oxide layer provides passivation, ensuring the material's longevity in construction and aerospace applications (Paz Martínez-Viademonte *et al.*, 2020; Al-Alimi *et al.*, 2024). However, in aggressive or specialized chemical environments, localized corrosion can lead to catastrophic structural failure and high maintenance costs. Environmentally, the impact is complex: while the stable oxide itself is benign, the leaching of aluminum ions under certain conditions (such as acid rain) can lead to aluminum toxicity in aquatic life and soils, posing an ecological threat (Ghazoui *et al.*, 2014; Hajjaji *et al.*, 2019).

Aluminum and its alloys are indispensable in modern industry due to their unique combination of properties, which make them suitable for a wide range of applications. Aluminum has a low density (2.7 g·cm^{-3}), making it ideal for applications requiring lightweight materials. Its alloys can achieve high strength-to-weight ratios, improve fuel efficiency and reduce emissions (Langelandsvik, 2021).

Aluminum holds the second position among metals in terms of production and use after steel. Aluminum is the most produced non-ferrous metal, surpassing others like copper and zinc in terms of production scale and economic importance (Valiev *et al.,* 2020). Aluminum is 100% recyclable, and recycled aluminum requires only 5% of the energy needed for primary production. This makes it a key material in sustainable manufacturing and circular economies (Peng *et al.,* 2022). This highlights its critical role in modern industry. Its versatility, combined with its environmental benefits, ensures its continued importance in addressing sustainability and technological advancement challenges.

Nevertheless, aluminum, like most industrially essential metals, is susceptible to corrosion. From a chemical standpoint, aluminum presents a double challenge for corrosion specialists. Due to its amphoteric properties, it can easily dissolve not only in acidic but also in alkaline solutions. **Table 1** represents a comparative description of the processes of aluminum dissolution in acids and bases.

Table 1. Comparative characteristics of aluminum corrosion processes in acidic and alkaline solutions

Features	**Corrosion in Acids**	**Corrosion in Alkalis**
Reaction Products	$2Al + 6H^+ \rightarrow 2Al^{3+} + 3H_2\uparrow$	$2Al + 2OH^- + 6H_2O \rightarrow 2[Al(OH)_4]^- + 3H_2\uparrow$
Oxide Layer Behavior	Dissolves	Dissolves
Corrosion Rate	Moderate to high	Generally higher
Surface Damage	Pitting and uniform corrosion	Severe etching and roughening
Gibbs Free Energy (ΔG^0)	-10 to -40 kJ/mol (depending on the specific acid and conditions)	~-29.80 kJ/mol (pure aluminum in 1M NaOH)
Spontaneity	Spontaneous	Spontaneous

As shown in **Table 1**, the corrosion behaviour of aluminium in acidic and alkaline environments differs markedly owing to distinct mechanisms and variations in the stability of the protective oxide layer. Both environments have negative ΔG^0 values, indicating that aluminum corrosion is thermodynamically favorable and spontaneous in both cases. Alkaline environments generally lead to more aggressive corrosion. It highlights the need for corrosion inhibitors against the corrosion of aluminum and its alloys in both acidic and alkaline environments.

In recent decades, natural inhibitors have been widely used for these purposes. Since environmental regulations have recently restricted the use of chemical inhibitors, plant extracts have regained importance as a renewable and environmentally friendly source of many essential inhibitors (El-Etre, 1998, 2005; Hmamou *et al.*, 2012; El Azzouzi *et al.*, 2022). The use of plant-based corrosion inhibitors is an important step towards sustainable development and the reduction of the environmental impact of harmful chemicals, making them promising candidates for industrial-scale use.

The western region of Kazakhstan is widely known for its plant biodiversity. There are more than 1,500 plant species representing more than 700 families. *G. uralensis* is one of the most widespread and strategically important plants for the region. Investigating the anticorrosive properties of *G. uralensis* extracts is a promising approach, as these extracts offer an environmentally friendly and effective method for protecting metals.

The current study uses weight-loss and potentiodynamic polarization techniques to investigate the inhibitory effect of *G. uralensis* aqueous extracts on the corrosion of D16T aluminum alloy in 0.1 $mol \cdot dm^{-3}$ NaOH solution. The kinetic and thermodynamic parameters of the corrosion process were evaluated. The aim of this work was also to assess the effects of the spring flood of 2024 on the anti-corrosion properties of *G. uralensis* extracts obtained from the whole plant and plant parts (roots, stems, leaves, and flowers).

2. Methodology

2.1 Reagents and solvents

All analytical grade reagents were used without any further purification. Double-distilled water (DDW) was used for the extraction and preparation of the corrosion media.

2.1.1 Plant collection

The 2023 and 2024 plant samples were collected in their natural habitat in the flowering stage in the suburbs of Uralsk at the same location in the first decade of July. The plant species were confirmed in the Herbarium of M. Utemisov West Kazakhstan University's Faculty of Natural and Geographical Sciences. The plant was air-dried in a shaded place for two weeks after being thoroughly washed with tap water and twice with DDW. After fine powder grinding and 1.0 mm sieve, samples were kept at 4°C for storage.

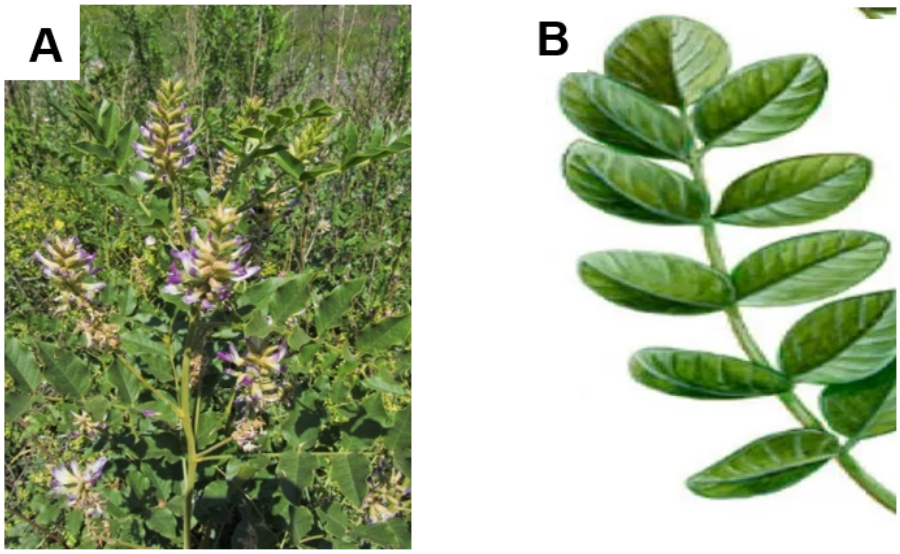

Figure 1: *G. uralensis whole plant* (A), and the appearance of *G.uralensis* leaves (B).

2.1.2 Preparation of the extract

10 g of dried and ground plant material were transferred into a 250 ml Erlenmeyer flask and extracted three times in a water bath with 100 ml of DDW at 60°C for 6 hours. A temperature accuracy of ± 0.1°C was maintained using a TW-2.02 water thermostat. The extracts were then combined and evaporated. After being dried to constant weight at 50°C extracts were kept in dark, sealed vials at 4°C until further use for anti-corrosion tests.

2.1.3 Metal preparation

Aluminum alloy D16T with composition of (wt.%): 92.7% - Al; Cu – 4.6%; Mg – 1.6%; Mn – 0.6%; Fe –0.19%; Si - 0.17%; Zn –0.07%; and dimensions of 25.0 x 30.0 x 3.0 mm were obtained from industry and used for corrosion tests. Prior to the experiment specimens were sequentially polished with emery paper ranging in grit numbers from 250 to 1200. Then, they were placed in an alkaline solution (40 g of NaOH per 1 liter of deionized water) for 10 sec, then rapidly rinsed in DDW, well dried in an air stream and isolated from the external atmosphere for further use.

2.2 Corrosion Study

2.2.1 Weight loss (gravimetric) method

Weight loss experiments were carried out to evaluate corrosion rate (CR), inhibitory effect (IE), and degree of surface coverage (θ). After pretreatment and weighting, the metal specimens were placed in an alkaline solution (40 g NaOH per 1.0 dm^3 of deionized water) for 10 seconds to remove the oxide film, rinsed with DDW, and immediately transferred to a 150 ml beaker containing 100 ml of corrosion medium with and without inhibitor. After the immersion time, the specimens were withdrawn from the beaker, and the corrosion products were removed by washing each coupon in a nitric acid solution (1:1) for 5 min at room temperature (ISO, 2021). The specimens were then washed again under running water, rinsed with ethanol and acetone, and dried before weighing again (Salim *et al.,* 2024): . All weight measurements were carried out with the Ohaus Adventurer Pro AV264 analytical balance with an accuracy of ±0.1 mg.

The corrosion rate (*CR* $g \cdot m^{-2} \cdot h^{-1}$), inhibition efficiency (IE_{wl}%), and degree of surface coverage (θ) were calculated according to the following **Eqns 1–3,** respectively:

$$CR(g \cdot m^{-2} \cdot h^{-1}) = \frac{\Delta m}{S \cdot \tau} \quad \textbf{Eqn. 1}$$

$$IE_{wl}(\%) = \frac{CR_0 - CR_i}{CR_0} \cdot 100 \quad \textbf{Eqn. 2}$$

$$\theta = \frac{IE_{wl}(\%)}{100} \quad \textbf{Eqn. 3}$$

where Δ*m* is the weight loss of the coupon (g) after the immersion period (h), S is the surface area of the specimen (m^2), CR_0 is the corrosion rate of aluminum alloy without inhibitor, and CR_i is the corrosion rate of aluminum alloy in the presence of the inhibitor.

2.3 Activation parameters calculations

The effect of temperature on the corrosion rate of D16T aluminium alloy in 0.1 $mol \cdot dm^{-3}$ NaOH solution in the presence and absence of the inhibitor was calculated using the Arrhenius equation (Seilova *et al.,* 2024):

$$\log \frac{CR_2}{CR_1} = \frac{E_a}{2.303R} \cdot \left(\frac{1}{T_1} - \frac{1}{T_2} \right) \quad \textbf{Eqn. 4}$$

where CR_1 and CR_2 – corrosion rates of D16T aluminium alloy ($g \cdot m^{-2} \cdot h^{-1}$) at T_1 and T_2 respectively, E_a – activation energy, R – universal gas constant (8.314 $J \cdot mol^{-1} \cdot K^{-1}$).

2.4 Absorption and thermodynamics

To determine the thermodynamic parameters and describe the inhibitor adsorption mechanism, different adsorption models are used. These models have their own mathematical expressions and graphical representations, and help to understand the nature of the interaction between inhibitor molecules and the metal surface. The Langmuir, Temkin, Frumkin, Freundlich, Flory-Huggins and El-Awady models are widely used for these purposes (Bazzi *et al.,* 2023; Loukili *et al.,* 2023; Salim *et al.,* 2024; Akatyev *et al.,* 2025;). In our research, we evaluated the applicability of all the above models to the adsorption of *G.uralensis* aqueous extracts on the surface of D16T aluminum alloy. In the following equations C_{inh} denote inhibitor concentration ($g \cdot dm^{-3}$), θ is degree of surface coverage, and K_{ads} is the equilibrium constant for absorption-desorption processes:

The Langmuir adsorption isotherms:

$$\frac{C_{inh}}{\theta} = \frac{1}{K_{abs}} + C_{inh} \quad \textbf{Eqn. 5}$$

The Temkin adsorption isotherms

$$\theta = \ln C_{inh} + K_{ads} \quad \textbf{Eqn. 6}$$

The Freundlich adsorption isotherms

$$\log\theta = \log K_{abs} + \frac{1}{n}\log C_{inh} \quad \textbf{Eqn. 7}$$

where *n* is a dimensionless constant indicating the intensity of the adsorption process.

The Flory-Huggins adsorption isotherms

$$\log\frac{\theta}{C_{inh}} = b\log(1-\theta) + \log K_{ads} \quad \textbf{Eqn. 8}$$

where *b* is the parameter representing the interaction between the adsorbate and the adsorbent.

The Frumkin adsorption isotherms

$$\log\left[C_{inh}\left(\frac{\theta}{1-\theta}\right)\right] = 2\alpha\theta + 2.303\log K_{ads} \quad \textbf{Eqn. 9}$$

where α is the interaction parameter that quantifies the interactions between adsorbed molecules on the surface.

The El-Awady adsorption isotherms

$$\log\left(\frac{\theta}{1-\theta}\right) = y\log C_{inh} + \log K$$

$$K_{ads} = K^{\frac{1}{y}} \quad \textbf{Eqn. 10}$$

where *y* - parameter represents the number of active sites occupied by one molecule of the inhibitor on the metal surface.

The values of the K_{ads} obtained from the above isotherm were used to calculate the Gibbs free energy according to the known relationship:

$$\Delta G^{0}_{abs} = -RT\ln(55.5K_{abs}) \quad \textbf{Eqn. 11}$$

ΔG^{0}_{ads} is the Gibbs free energy of absorption, *R* is the universal gas constant (8.314 $J\cdot K^{-1}\cdot mol^{-1}$), T is the system's thermodynamic temperature, and 55.5 is the molar concentration of water $mol\cdot dm^{-3}$.

The heat of absorption (Q_{ads}) of the inhibitor on the metal surface was obtained for the trend of surface coverage with temperature using the following equation:

$$Q_{abs} = 2.303R\left(\log\frac{\theta_2}{1-\theta_2} - \log\frac{\theta_1}{1-\theta_1}\right)\cdot\left(\frac{T_1\cdot T_2}{T_2 - T_1}\right) \quad \textbf{Eqn. 12}$$

2.5 Electrochemical measurement

The same pretreatment was applied to the alloy specimens for the electrochemical experiment as for the weight loss test. The Autolab PGSTAT 101 Metrohm potentiostat/galvanostat, equipped with the NOVA 2.1.8 software, was used for the electrochemical test. A three-electrode setup was used to electrochemical measurements: reference electrode (Ag/AgCl filled with 3.0 $mol\cdot dm^{-3}$ KCl), counter

electrode (platinum), and working electrode (alloy specimen). A beaker containing 100 ml of 3% NaCl, both with and without inhibitor, served as the electrochemical cell. The working electrode, with an exposed area 1.0 cm^2 was stabilized during open circuit potential (OCP) testing. The linear sweep voltammetry (LSV) staircase and corrosion rate analysis were used to perform linear polarization measurements right after the OCP. Potentiodynamic scanning was performed with a scan rate of 0.01 V/s between -0.50 and +0.50 V. From the Tafel polarization curves, the corrosion potential (E_{corr}) and corrosion current density (j_{corr}) were established.

Formula 13 was used to obtain the inhibition efficiency (IE_i%) through the corrosion current (Li *et al.,* 2023; Arrousse *et al*., 2020):

$$IE_i(\%) = \frac{i_{inh} - i_{corr}}{i_{inh}} \cdot 100 \qquad \textbf{Eqn. 13}$$

where i_{inh} and i_{corr} are the corrosion current densities determined by extrapolating the Tafel slopes with and without inhibitors, respectively, $A \cdot cm^{-2}$.

Using the equation (14), the inhibition efficiency through the polarization resistance (IE_R%) was determined (Liu *et al.,* 2010):

$$IE_R(\%) = \frac{R_p^{inh} - R_p^0}{R_p^{inh}} \cdot 100 \qquad \textbf{Eqn. 14}$$

where R_p^{inh} and R_p^0 represent the charge-transfer resistances with and without the inhibitor, respectively, in Ω.

2.6 Contact angle measurement

Hydrophilicity of the alloy coupons was assessed by measuring the contact angle between a water drop and the alloy surface using the Ossila Contact Angle Goniometer equipped by the Ossila Contact Angle software *ver.* 4.2.0. The drops of water were mounted on the surface of alloy sample using a micro-syringe with needle diameter of 0.4 mm. The reported contact angles were an average of at least three measurements on different areas of the surface. Photos of water drops were obtained using a high-resolution video camera and the above software.

3. Results and Discussion

3.1 Weight loss assay

At the beginning of our study, a weight loss analysis was performed to determine which part of the *G. uralensis* plant is most effective as a corrosion inhibitor of D16T aluminum alloy in 0.1$mol \cdot dm^{-3}$ NaOH solution in 2023 and 2024. The results are presented in **Table 2.** As shown in **Figure 2**, at the same concentration in a given alkaline environment, the inhibition efficiency of aqueous extracts of *G. uralensis* parts decreases in the order of leaves > flowers > stems > roots > whole plant in 2023, and leaves > flowers > stems > whole plant > roots in 2024. Extracts obtained from the leaves demonstrated the best inhibitory properties in both 2023 and 2024 (56.38% and 71.26% respectively). Moreover, the inhibition efficiency of leaf extracts increased significantly in 2024. At the same time, the anticorrosive properties of all other parts and the whole plant remain at the same level. In addition, to confirm the results of the weight loss assay, electrochemical measurements were performed. The OCP *versus* time diagram and Tafel polarization curves for different parts of *G. uralensis* plant for D16T aluminum alloy in 0.1 $mol \cdot dm^{-3}$ NaOH at 1.0 $g \cdot dm^{-3}$ inhibitor concentration at room temperature are shown in **Figure 3.** The results obtained from the electrochemical experiment are shown in **Table 3.**

Table 2. Corrosion parameters obtained from the weight loss test of aluminum alloy D16T in 0.1 mol·dm^{-3} NaOH solution with 1.0 g·dm^{-3} aqueous extracts of *G. uralensis* parts for a 6-hour immersion time at room temperature.

Plant part	Time, h	CR, g·m^{-2}·h^{-1}	IE$_{wl}$%	θ	CR, g·m^{-2}·h^{-1}	IE$_{wl}$%	θ
		2023			2024		
Blank	2	20.47	-	-	20.47	-	-
	4	22.79	-	-	22.79	-	-
	6	26.38	-	-	26.38	-	-
	8	31.92	-	-	31.92	-	-
Whole plant	2	17.73	13.38	0.1338	16.43	19.73	0.1973
	4	18.54	18.62	0.1862	17.32	23.97	0.2397
	6	19.72	25.24	0.2524	18.79	28.76	0.2876
	8	20.48	35.85	0.3585	19.69	38.32	0.3832
Roots	2	17.99	12.11	0.1211	17.65	13.77	0.1377
	4	18.52	18.71	0.1871	18.32	19.58	0.1958
	6	19.93	24.44	0.2444	19.56	25.84	0.2584
	8	20.08	37.10	0.3710	20.94	34.41	0.3441
Steams	2	12.27	40.06	0.4006	11.45	44.06	0.4406
	4	13.20	42.06	0.4206	12.01	47.28	0.4728
	6	14.01	46.88	0.4688	13.07	50.45	0.5045
	8	15.43	51.67	0.5167	14.24	55.39	0.5539
Leaves	2	11.87	41.99	0.4199	7.87	61.56	0.6156
	4	12.04	47.15	0.4715	8.15	64.21	0.6421
	6	12.38	53.05	0.5305	8.85	66.46	0.6646
	8	13.93	56.38	0.5638	9.18	71.26	0.7126
Flowers	2	12.82	37.37	0.3737	12.06	41.08	0.4108
	4	13.32	41.53	0.4153	12.16	46.62	0.4662
	6	13.69	48.09	0.4809	13.03	50.60	0.5060
	8	14.76	53.77	0.5377	14.12	55.77	0.5577

The results of the electrochemical experiment are in complete agreement with the weight loss assay. Reduction of the corrosion current to a minimum value and a corresponding increase in polarization resistance unequivocally confirm that *G. uralensis* leaves aqueous extracts have the best inhibitory properties. Based on the results obtained, the leaf extracts were selected for further detailed research. At the next stage of our study, the inhibition efficiency of D16T aluminum alloy in 0.1mol·dm^{-3} NaOH solution with *G. uralensis* leaves aqueous extracts was evaluated at various

inhibitor concentrations. **Figure 4** shows the effect of the concentration of *G. uralensis* leaves aqueous extracts on CR and IE for D16T aluminum alloy in 0.1 mol·dm^{-3} NaOH solution.

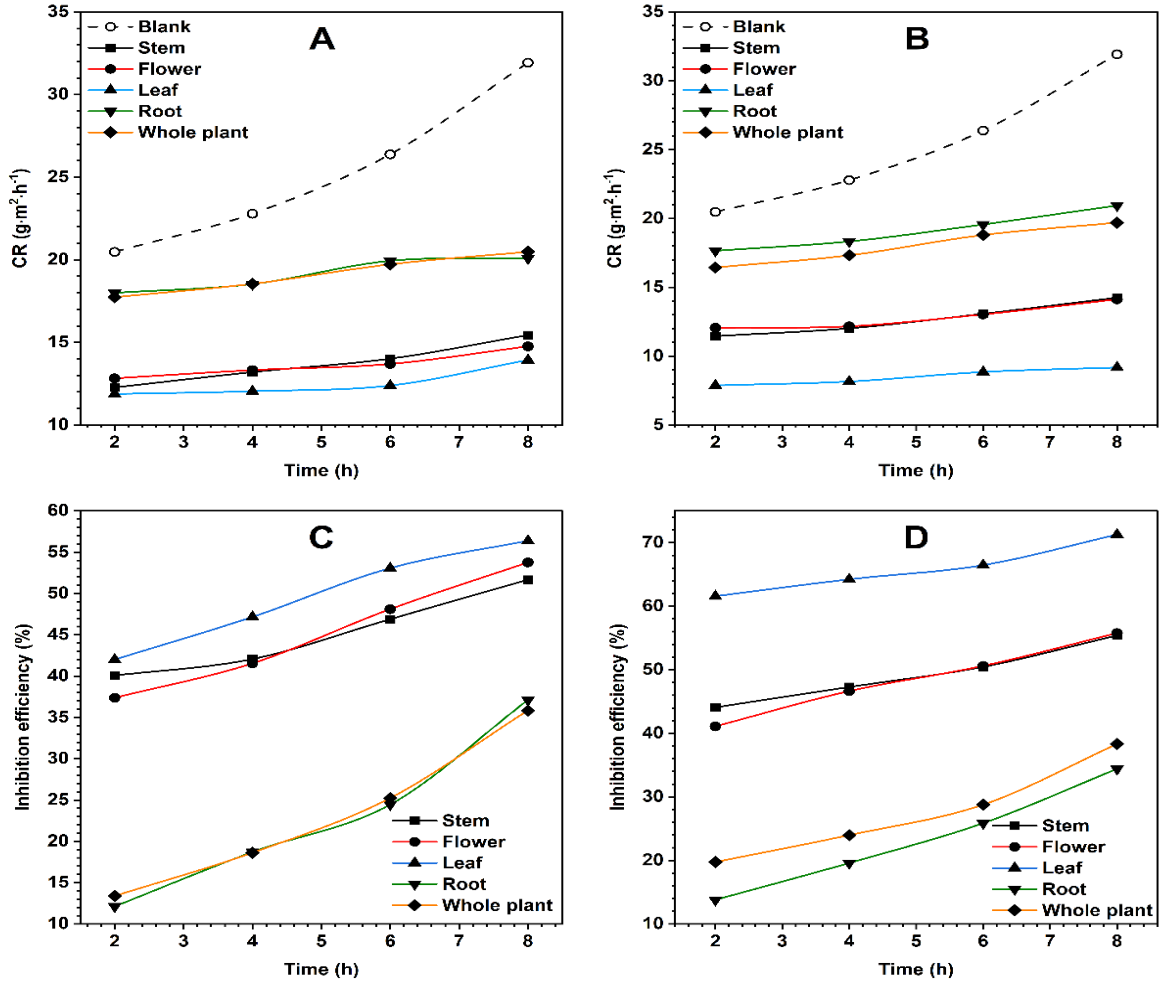

Figure 2. Corrosion rate (CR) (A – 2023, B - 2024) and inhibition efficiency (IE_{wl}) (C – 2023, B - 2024) for *G. uralensis* aqueous extracts (1.0 g·dm^{-3}) in 0.1 mol·dm^{-3} NaOH solution for a 6-hour immersion time at room temperature.

Table 3. The electrochemical parameters of D16T aluminum alloy in 0.1 mol·dm^{-3} NaOH with and without *G. uralensis* plant parts aqueous extracts (1.0 g·dm^{-3}) at room temperature.

C_{inh}, g·dm^{-3}	-E_{corr}, mV	J_{corr}, A·cm^{-2}	IE_i, %	$\|b_a\|$, mV·dec^{-1}	$\|b_c\|$, mV·dec^{-1}	Rp, Ω	IE_R, %
Blank	1544.6	$5.65\cdot10^{-4}$	-	105.62	126.25	44.18	-
			2023				
Whole plant	1476.1	$4.85\cdot10^{-4}$	14.07	107.02	96.76	51.23	13.76
Roots	1496.6	$4.40\cdot10^{-4}$	22.00	97.59	89.23	50.90	13.21
Stems	1479.0	$5.04\cdot10^{-4}$	10.87	75.12	69.50	56.87	22.34
Leaves	1449.1	$3.96\cdot10^{-4}$	29.91	131.72	110.65	68.63	35.63
Flowers	1468.6	$4.09\cdot10^{-4}$	27.66	87.49	86.03	53.15	16.87
			2024				
Whole plant	1472.9	$3.28\cdot10^{-4}$	41.88	39.24	42.99	72.07	38.70
Roots	1476.4	$3.47\cdot10^{-4}$	38.57	91.39	86.65	78.03	43.39
Stems	1465.5	$2.94\cdot10^{-4}$	47.94	65.27	62.79	68.03	35.06
Leaves	1439.2	$2.58\cdot10^{-4}$	54.24	111.44	101.58	83.31	46.97
Flowers	1466.8	$3.58\cdot10^{-4}$	36.52	56.97	54.81	76.35	42.14

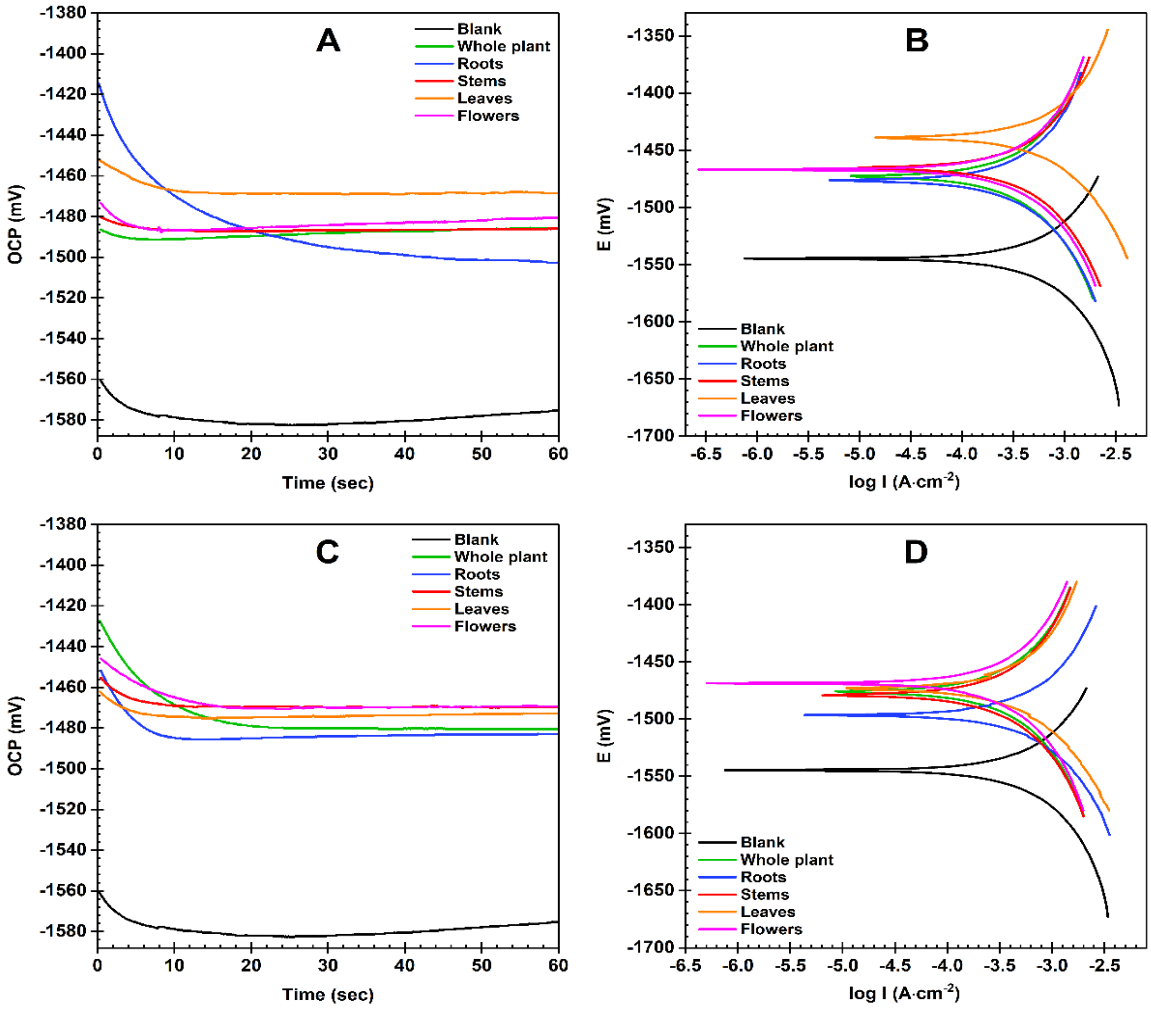

Figure 3. OCP *vs.* time (A – 2023, C - 2024) and Tafel polarization curves (B – 2023, D - 2024) for D16T aluminum alloy in 0.1 mol·dm^{-3} NaOH with and without *G. uralensis* plant parts aqueous extracts (1.0 g·dm^{-3}) at room temperature

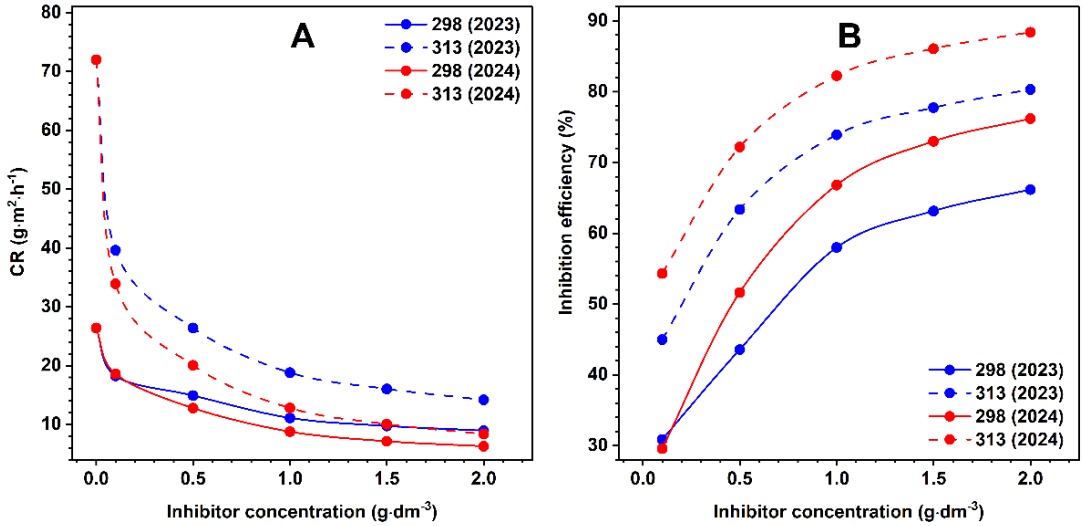

Figure 4. The relationship between CR (A) and IE (B) of *G.uralensis* leaves aqueous extracts, in 2023 and 2024, for D16T aluminum alloy in 0.1 mol·dm^{-3} NaOH solution at various concentrations of the inhibitor and immersion time at 298 and 313 K.

The corrosion rate (CR), inhibition efficiency (IE_{wl}), and degree of surface coverage (θ) obtained from weight loss analysis for D16T aluminum alloy in 0.1 mol·dm^{-3} NaOH solution at 298 and 313 K in the absence and presence of *G. uralensis* leaves aqueous extract are listed in **Table 4.**

Table 4. Corrosion parameters of D16T aluminum alloy in 0.1 mol·dm^{-3} NaOH solution at presence of various concentrations of *G.uralensis* leaves aqueous extracts for a 6-hour immersion time at 298 and 313 K

T, K	C_{inh}, g·dm^{-3}	CR, g·m^{-2}·h^{-1}	IE_{wl}%	θ	CR, g·m^{-2}·h^{-1}	IE_{wl}%	θ
		2023			2024		
298	Blank	26.38	-	-	26.38	-	-
	0.1	18.24	30.84	0.3084	18.58	29.56	0.2956
	0.5	14.89	43.55	0.4355	12.76	51.61	0.5161
	1.0	11.08	57.98	0.5798	8.76	66.81	0.6681
	1.5	9.73	63.13	0.6313	7.13	72.98	0.7298
	2.0	8.93	66.16	0.6616	6.28	76.20	0.7620
313	Blank	71.98	-	-	71.98	-	-
	0.1	39.61	44.97	0.4497	33.89	54.31	0.5431
	0.5	26.38	63.35	0.6335	20.03	72.17	0.7217
	1.0	18.79	73.90	0.7390	12.79	82.24	0.8224
	1.5	16.03	77.73	0.7773	10.03	86.06	0.8606
	2.0	14.17	80.31	0.8031	8.36	88.38	0.8838

As shown in Table 4, the aqueous extract of *G. uralensis* leaves significantly reduces the corrosion rate. The inhibitory effect of the D16T aluminum alloy in the presence of *G. uralensis* leaves aqueous extracts in a 0.1 mol·dm^{-3} NaOH solution depends on the inhibitor concentration and also increases with exposure time. It was found that the inhibitor provides the most effective corrosion inhibition at both temperatures at a concentration of 2.0 g·dm^{-3}. Therefore, for the best metal protection, the inhibitor should be used at higher concentrations. It was also found that the protective effect of aqueous extracts from the leaves of *G. uralensis* increased in 2024 compared to 2023 (80.31% and 88.38%, respectively). The results obtained suggest that the aqueous extract from *G. uralensis* leaves offers promising potential for preventing metal corrosion in alkaline solutions. Thus, the aqueous extract from *G. uralensis* leaves reduces the destruction of metal in a 0.1 mol·dm^{-3} NaOH solution, forming a protective layer on its surface.

3.2 Adsorption and thermodynamics

The inhibitor can adsorb on the metal surface by a chemical, physical, or combined way. Determining the values of the Gibbs free energy of adsorption (ΔG^0_{ads}) is necessary to characterize the adsorption mechanism and determine the adsorption nature. The electrostatic interaction (physisorption) between charged inhibitor molecules and metal surfaces is represented by ΔG^0_{ads} values up to -20 kJ·mol^{-1}. A value less than or equal to about -40 kJ·mol^{-1}, commonly considered the threshold between chemisorption and physisorption, indicates the chemical character of the sorption (Miralrio and Espinoza Vázquez, (2020).

Adsorption isotherms for *G. uralensis* leaves aqueous extract on D16T aluminum alloy surface in a 0.1 mol·dm^{-3} NaOH solution for 2023 and 2024 at 298 and 313K are given in **Figure 5.**

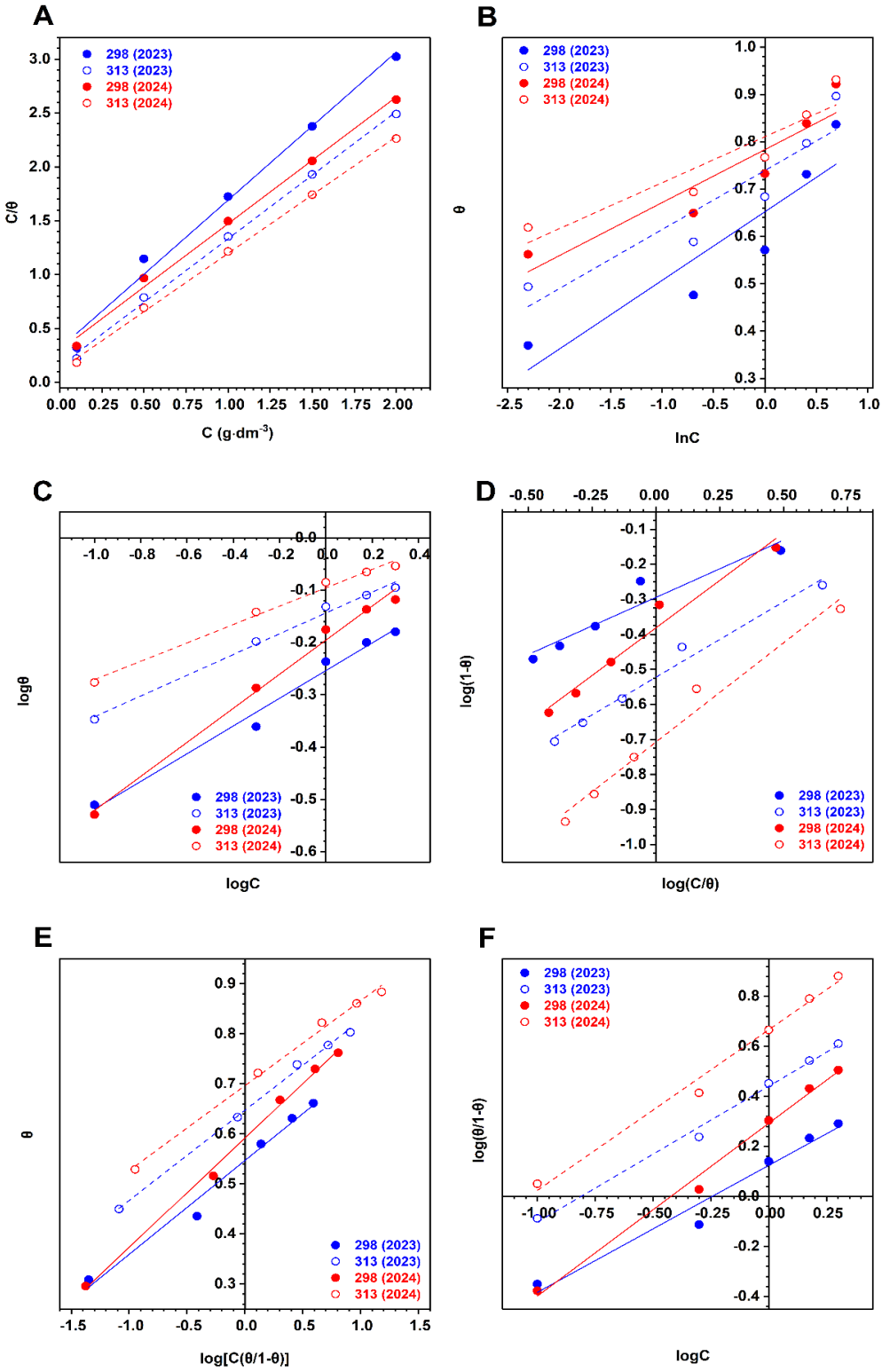

Figure 5. Adsorption isotherms for *G. uralensis* leaves aqueous extract on D16T aluminum alloy in 0.1 mol·dm^{-3} NaOH solution for 2023 (blue lines) and 2024 (red lines), at 298 (solid lines) and 313K (dashed lines) for 2 hours immersion period: A - Langmuir, B - Temkin, C - Freundlich, D - Flory-Huggins, E - Frumkin, F - El-Awady

The Gibbs free energy (ΔG^0_{ads}) and K_{ads} values for the aqueous extract of *G. uralensis* leaves were determined based on the slopes and intercepts of the linear plots in accordance with **Eqns 5-10.** **Table 5** presents the thermodynamic parameters obtained.

Table 5. Thermodynamic parameters of adsorption of *G. uralensis* leaves aqueous extract on D16T aluminum alloy surface in 0.1 mol·dm^{-3} NaOH solution.

Isotherm	T, K	Slope	Intercept	R^2	K_{ads}	ΔG^0_{ads}, kJ·mol^{-1}	Isotherm property
				2023			
Langmuir	298	1.37496	0.31681	0.99078	3.16	-12.80	-
	313	1.18061	0.15280	0.99830	6.54	-15.34	-
				2024			
	298	1.17588	0.29743	0.99562	3.36	-12.96	-
	313	1.08334	0.11474	0.99870	8.72	-16.09	-
				2023			
Temkin	298	0.14508	0.65202	0.84291	0.65	-8.89	-
	313	0.12483	0.73918	0.86467	0.74	-9.67	-
				2024			
	298	0.11219	0.78348	0.86822	0.78	-9.35	-
	313	0.09722	0.81057	0.86710	0.81	-9.91	-
							n
				2023			
Freundlich	298	0.26472	-0.25388	0.99440	0.56	-8.50	3.78
	313	0.19842	-0.14357	0.99288	0.72	-9.59	5.04
				2024			
	298	0.32566	-0.19563	0.99182	0.64	-8.84	3.07
	313	0.17553	-0.09543	0.99088	0.80	-9.88	5.70
							b
				2023			
Flory-Huggins	298	0.32635	-0.29448	0.91721	0.51	-8.27	0.33
	313	0.43076	-0.52240	0.98209	0.30	-7.32	0.43
				2024			
	298	0.54278	-0.38171	0.96910	0.42	-7.77	0.54
	313	0.56690	-0.70770	0.97696	0.20	-6.21	0.57
							α
				2023			
Frumkin	298	0.18747	0.54669	0.99316	1.73	-11.31	0.094
	313	0.17999	0.64699	0.99780	1.91	-12.14	0.090
				2024			
	298	0.21821	0.59137	0.99705	1.81	-11.42	0.109
	313	0.16961	0.69644	0.99502	2.01	-12.27	0.085
							1/y
				2023			
El-Awady	298	0.50734	0.12389	0.96862	1.33	-14.06	3.94
	313	0.54324	0.44060	0.98378	2.76	-16.49	3.68
				2024			
	298	0.69055	0.29208	0.96216	1.96	-14.25	2.90
	313	0.64188	0.66640	0.98929	4.64	-17.41	3.12

Negative values of ΔG^0_{ads} indicate that the absorption of the aqueous extract of *G. uralensis* leaves on the surface of the D16T aluminum alloy is a spontaneous process (Nwabanne and Okafor (2012). The value of $\Delta G^0_{ads} > -20$ kJ·mol^{-1} clearly shows that the adsorption is physical (physisorption) and occurs as a result of the electrostatic interaction of charged inhibitor molecules with the alloy surface (Ostovari *et al.,* 2009). An increase in temperature and inhibitor concentration accelerates adsorption-desorption processes and promotes the formation of a stable protective barrier on the metal surface (Fouda *et al.,* 2016).

As shown, the adsorption of *G. uralensis* leaves aqueous extracts can be described by several isotherms, in particular the Langmuir, Freundlich, and Frumkin isotherms. The correlation coefficient (R^2) values greater than 0.99 indicate that all of these models are suitable for explaining the adsorption of the aqueous extract of G. uralensis leaves on the D16T aluminum alloy surface. The simultaneous adsorption of the inhibitor to several isotherms may occur due to the complexity of the adsorption processes and the different nature of interactions at the metal-inhibitor interface.

The Langmuir isotherm suggests that the formation of the inhibitor protective layer occurs through the replacement of water molecules on the metal surface with inhibitor molecules, which are adsorbed from the solution (Nailya *et al.,* 2018). This can be attributed, for instance, to the higher dipole moment of the inhibitor molecules, which results in adsorption forces that are noticeably stronger than those of water molecules on the metal surface.

The applicability of the Freundlich isotherm indicates that adsorption occurs on a heterogeneous surface with varying adsorption energies, implying that the metal surface has sites with different affinities for the inhibitor molecules. The heterogeneity of a metal surface, which leads to different adsorption energies and sites with varying affinities for inhibitor molecules, can be explained by microscopic irregularities, pits, cracks, and grain boundaries that create regions with different surface energies (Loto, 2022). Moreover, metals and alloys consist of grains with different crystallographic phases, each with distinct atomic arrangements and surface energies, leading to variations in inhibitor adsorption affinity and a combination of isotherms.

The Frumkin isotherm accounts for lateral interactions between adsorbed molecules, suggesting that adsorption is influenced by attractive or repulsive forces among adsorbed species (Aransiola, 2023). Therefore, the application of three adsorption models implies a complex adsorption process involving both uniform and non-uniform surface characteristics, the formation of multilayers of the inhibitor as well as interactions between adsorbed inhibitor molecules.

It was also found that the adsorption of extracts obtained from both plant samples from 2023 and 2024 obeys the same isotherms. Considering that the 2024 samples exhibit better anti-corrosion properties than the 2023 samples, this suggests that the content of bioactive compounds in plants has increased, while the types of phytocomponents responsible for adsorption remain the same. Therefore, these compounds similarly interact with the metal surface, resulting in the identical adsorption behavior (Umoren *et al.,* 2007).

Table 6 presents the values of activation energy (E_a) and heat of adsorption (Q_{ads}) calculated with **Eqns 4 and 12**, respectively.

Table 6. Activation energy (E_a) of the dissolution of D16T aluminum alloy and heat of adsorption (Q_{ads}) of *G. uralensis* leaves aqueous extract in 0.1 mol·dm^{-3} NaOH.

C_{inh}, g·dm^{-3}	E_a, kJ·mol^{-1}		Q_{ads}, kJ·mol^{-1}	
	2023	2024	2023	2024
0.0	51.95	51.95	-	-
0.1	40.14	38.19	51.51	53.84
0.5	29.60	23.34	41.71	45.94
1.0	27.34	19.06	37.17	43.08
1.5	25.84	17.66	36.83	42.75
2.0	23.90	14.81	38.02	44.74

The graphical representation of the relationship between activation energy (E_a) and heat of adsorption (Q_{ads}) of the inhibitor for 2023 and 2024 is given in **Figure 6.**

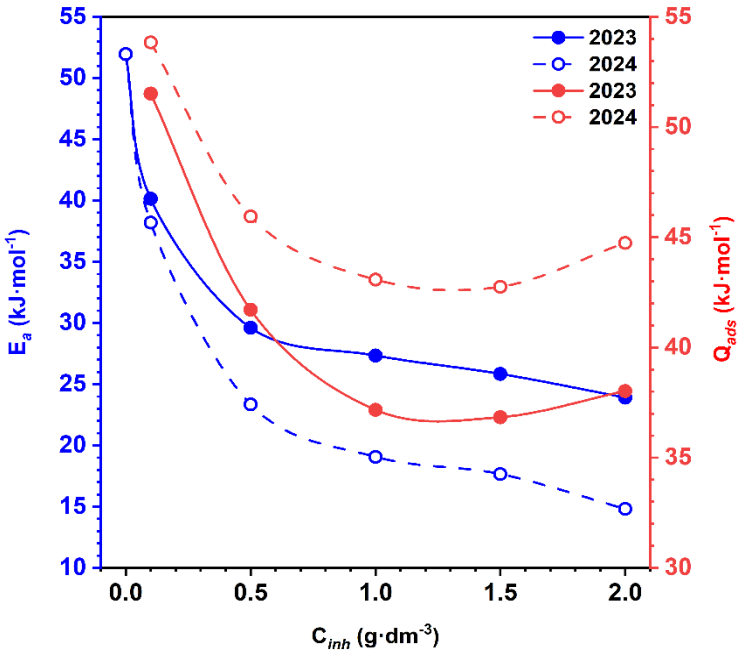

Figure 6. Activation energy (E_a) (blue lines) and heat of adsorption (Q_{ads}) (red lines) of the dissolution of D16T aluminum alloy in 0.1 mol·dm^{-3} NaOH in the presence and absence of *G. uralensis* leaves aqueous extract for 2023 (solid lines) and 2024 (dashed lines).

As can be seen, the activation energy in the presence of aqueous extract of *G. uralensis* leaves is lower than in an uninhibited 0.1 mol·dm^{-3} NaOH solution. The values of $E_a < 80$ kJ·mol^{-1} indicate that the adsorption is of a physical nature (physisorption). The decrease in the activation energy of the corrosion process with increasing inhibitor concentration indicates a better surface coverage and more effective corrosion inhibition. An increase in the inhibitor concentration leads to a decrease in the values of both parameters. A reduction in activation energy reflects a simultaneous decrease in the adsorption energy barrier, thereby enhancing the anticorrosive efficiency. Moreover, increasing both the temperature and the inhibitor concentration accelerates the attainment of equilibrium in the adsorption–desorption processes, favoring the formation and stabilization of a protective film on the aluminum alloy surface (Fouda *et al.*, 2016). The changes in both parameters for the 2023 and 2024 samples show the same trend, but the values are different. The activation energy for the 2024 samples is lower than for 2023, while the heat of adsorption of the inhibitor for the 2024 samples exceeds the same values for 2023. Obviously, these changes are also associated with alterations in the phytochemical composition of the examined extracts.

3.3 UV–visible spectroscopy analysis

UV–Visible spectroscopy is a powerful analytical technique widely used to investigate the electronic properties of coordination compounds. It provides valuable information on metal–ligand interactions and charge-transfer transitions, offering insights into the nature of bonding, the geometry of complexes, and the oxidation state of the metal center. This makes it an essential tool for understanding the electronic structure and reactivity of coordination systems. To confirm that the protective effect of 2 years is due to the adsorption of the aqueous extract of G. uralensis leaves onto the surface of the aluminum alloy, UV-Vis spectrometric analysis of the corrosion environment was performed. UV-visible spectra were recorded before and after immersion of the D16T aluminum alloy specimens for 8 hours in the presence of 0.5 g·dm^{-3} of the inhibitor (**Figure 7**).

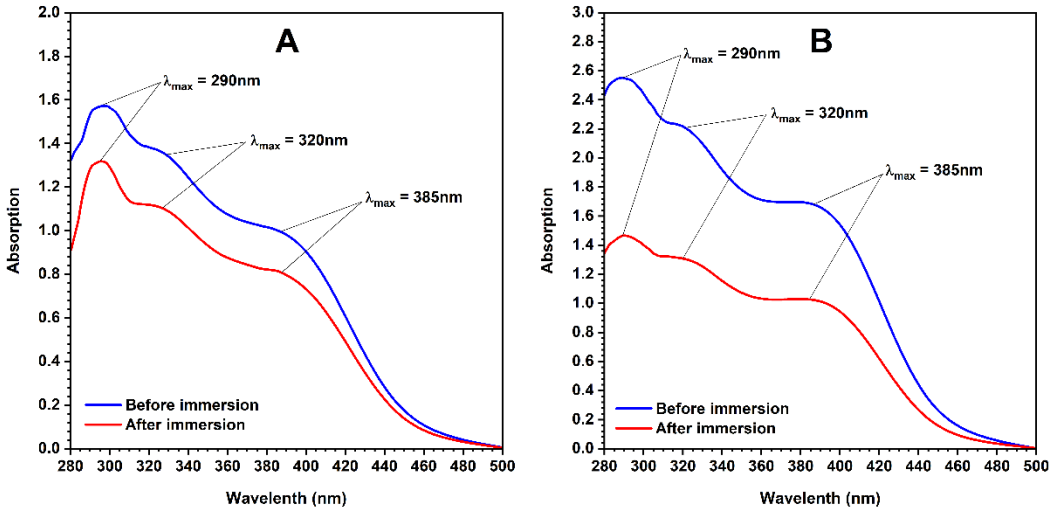

Figure 7. UV-Vis-spectra of *G. uralensis* leaves aqueous extracts in 0.1 mol·dm^{-3} NaOH solution before (blue line) and after (red line) 8 hours immersion of D16T aluminum alloy for 2023 (A) and 2024 (B).

As can be seen, the UV-visible spectrum of the solution before and after immersion demonstrates absorption maxima at 290, 320, and 385 nm, which is typical for phenolic phytocomponents (Akatyev and Samigolla, (2024). It is obvious that the absorption is due exclusively to the components of the studied extract. However, after immersion of the metal sample in a corrosive environment in the presence of 0.5 g dm^{-3} of the inhibitor for 8 hours, the absorption intensity decreases significantly. In addition, no shifts in the maximum absorption values were observed in the UV-visible spectra, which indicates the absence of any chemical interactions of the extract components with either the corrosion environment or metal ions. The strong hypochromic effect observed after immersion of the metal sample is due to a decrease in the concentration of the corresponding phytocomponents in solution, resulting from their adsorption onto the metal surface. Other phenomena, such as turbidity or sediment formation, which could also lead to a similar effect, were not observed. Thus, UV-Vis spectroscopy analysis also confirms the adsorption of the inhibitor on the metal surface and its physical mechanism. These observations also suggest that the adsorbed phytocomponents are phenolic. A more pronounced hypochromic effect in the 2024 sample also indicates a higher inhibition efficiency.

The survey literature indicates that the aqueous extract of G. uralensis leaves contains various bioactive compounds, as shown in **Figure 8**. The presence of aromatic rings, double bonds, and heteroatoms, such as oxygen, facilitates adsorption on the metal surface, creating a barrier against the arrival of aggressive species such as H^+ and dissolved oxygen, which are responsible for the anodic reactions. The corrosion inhibitory action is generally interpreted by the synergistic intermolecular effect of the components at different contents as described by several authors (Khadraoui *et al.,* 2014; Al-Amiery *et al.,* 2023; Lrhoul *et al.,* 2023; Batah *et al.,* 2024; Bandeira *et al.,* 2025)

3.4 Electrochemical experiment

The OCP evaluation of the D16T aluminum alloy was carried out with and without aqueous extract *G. uralensis* leaves during a 60-second immersion in 0.1 mol·dm^{-3} NaOH solution. Figure 9 shows the corresponding OCP curves as a function of time and the Tafel polarization curves. Figures 9A and 9C show that the OCP reaches the equilibrium state before 60 s. The shift in the OCP value with different concentrations of the aqueous extract of *G. uralensis* leaves indicates that the inhibitor molecules were adsorbed on the alloy surface (El-Azabawy *et al*., 2023).

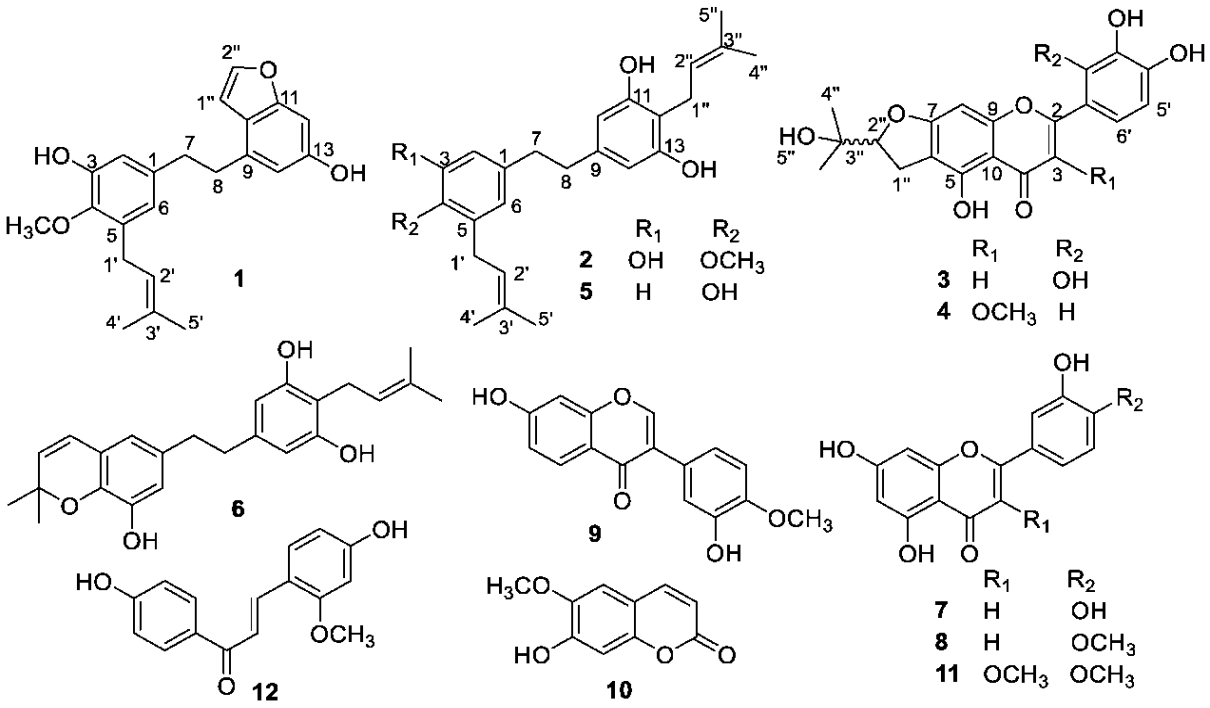

Figure 8. Biomolecules determined in *G. uralensis* leaves aqueous extract (Wang *et al.,* 2019).

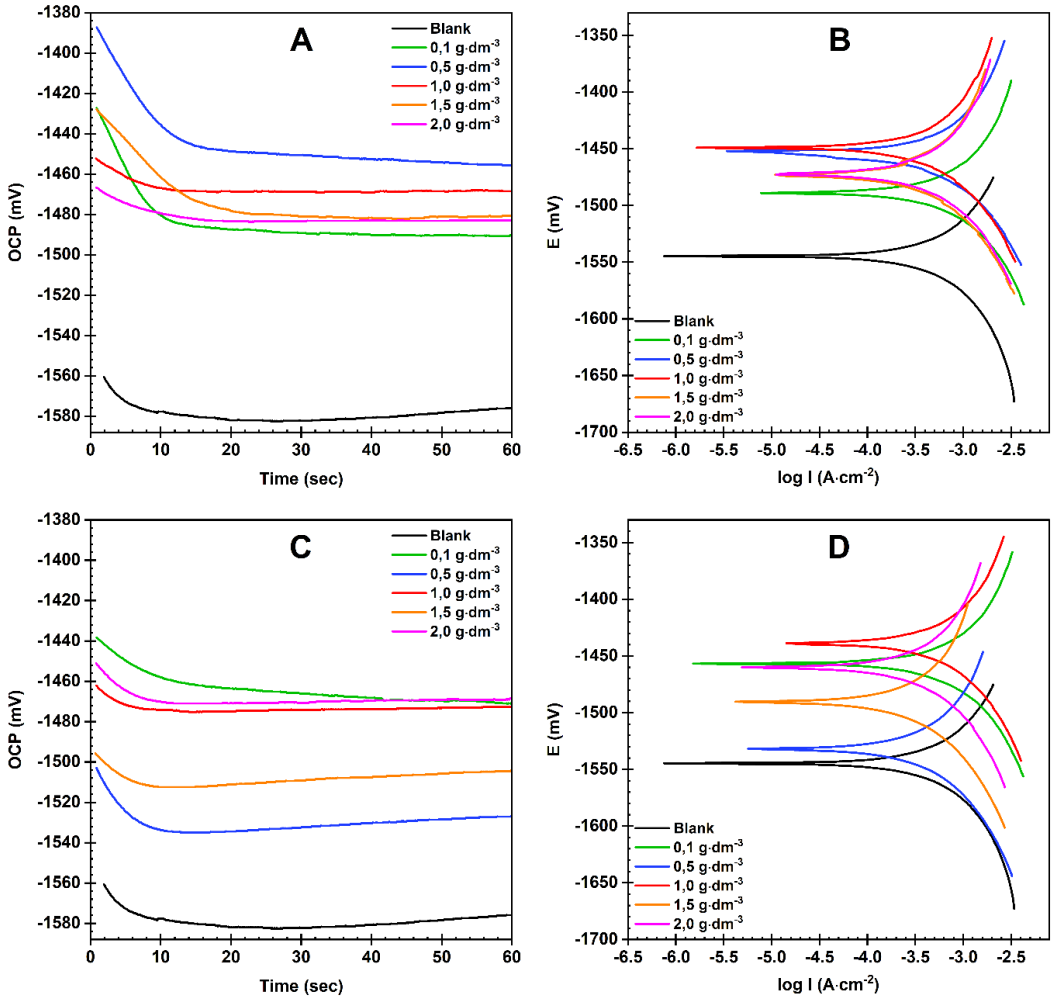

Figure 9. OCP *vs.* time (A – 2023, C - 2024) and Tafel polarization curves (B – 2023, D - 2024) for D16T Al alloy in 0.1 M NaOH at different concentrations of *G.uralensis* leaves aqueous extracts

Figures 9B, and 8D shows the potentiodynamic polarization curves for the D16T aluminum alloy in 0.1 mol·dm^{-3} NaOH solutions with and without of *G. uralensis* leaves aqueous extract. The electrochemical parameters of the corrosion process obtained from the polarization curves using corrosion rate analysis are shown in **Table 7.**

Table 7. The electrochemical parameters of D16T aluminum alloy in 0.1 mol·dm^{-3} NaOH at different concentrations of *G.uralensis* leaves aqueous extracts for 2023 and 2024.

C_{inh}, g·dm^{-3}	-E_{corr}, mV	J_{corr}, A·cm^{-2}	IE_i, %	$\|b_a\|$, mV·dec^{-1}	$\|b_c\|$, mV·dec^{-1}	R_p, Ω	IE_R, %
0.0	1544.6	$5.65\cdot10^{-4}$	-	105.62	126.25	44.18	-
			2023				
0.1	1488.9	$4.48\cdot10^{-4}$	10.78	129.12	106.57	52.00	15.05
0.5	1457.3	$3.47\cdot10^{-4}$	23.00	168.86	121.68	57.77	23.53
1.0	1449.1	$3.96\cdot10^{-4}$	29.91	131.72	110.65	68.63	35.63
1.5	1473.4	$1.80\cdot10^{-4}$	48.62	155.86	112.54	83.87	47.33
2.0	1472.3	$1.07\cdot10^{-4}$	63.21	164.31	123.06	97.80	54.83
			2024				
0.1	1456.7	$5.04\cdot10^{-4}$	20.73	112.40	100.95	65.63	32.69
0.5	1532.1	$4.35\cdot10^{-4}$	38.61	137.33	114.58	74.68	40.84
1.0	1439.2	$2.58\cdot10^{-4}$	54.24	111.44	101.58	83.31	46.97
1.5	1490.6	$2.90\cdot10^{-4}$	68.11	173.13	113.88	96.32	54.13
2.0	1460.2	$2.07\cdot10^{-4}$	80.92	138.22	107.86	125.13	64.69

The corrosion current density values (J_{corr}) are significantly lower in the presence of the inhibitor, indicating that the aqueous extract of *G. uralensis* leaves effectively protects the metal surface from corrosion (Raja and Sethuraman, (2008). The polarization resistance (R_p) increases with increasing inhibitor concentration, confirming the formation of a protective layer that prevents corrosion damage (Solmaz *et al.,* 2008). As shown, both the cathodic and anodic portions of the polarization curves shift noticeably in the presence of the inhibitor. Thus, the aqueous extract of *G. uralensis* leaves acts as a mixed-type inhibitor, slowing down both cathodic and anodic reactions (Tsygankova *et al.,* 2013; Ettahiri et al., 2024). However, the shifts of the cathodic region $|b_c|$ are greater than the anodic $|b_a|$, which means that the cathodic polarization is more susceptible to the influence of the inhibitor than the anodic one. In addition, in the presence of *G. uralensis* leaves aqueous extract, the inhibitory effect values determined from corrosion current and polarization resistance in accordance with equations 10 and 11 increased significantly with the increase of inhibitor concentration. This also indicates that the studied inhibitor has a high potential to prevent the corrosion of D16T aluminum alloy in 0.1 mol·dm^{-3} NaOH solution. The electrochemical and gravimetric data were found to be in excellent agreement.

3.5 Contact angle measurement

Contact angle measurements were performed to evaluate the formation and effectiveness of the protective film derived from the aqueous extract of *G. uralensis* leaves on the surface of D16T aluminum alloy. This technique enabled assessment of surface property changes, providing insight into changes in surface wettability and the presence of an adsorbed inhibitor layer. This experiment provides insight into the surface wettability and the effectiveness of the inhibitor. A higher contact angle indicates increased hydrophobicity, suggesting that the inhibitor forms a protective layer on the alloy surface, reducing its wettability and potentially improving corrosion resistance. The contact angles and droplet appearance are shown in **Figure 10.**

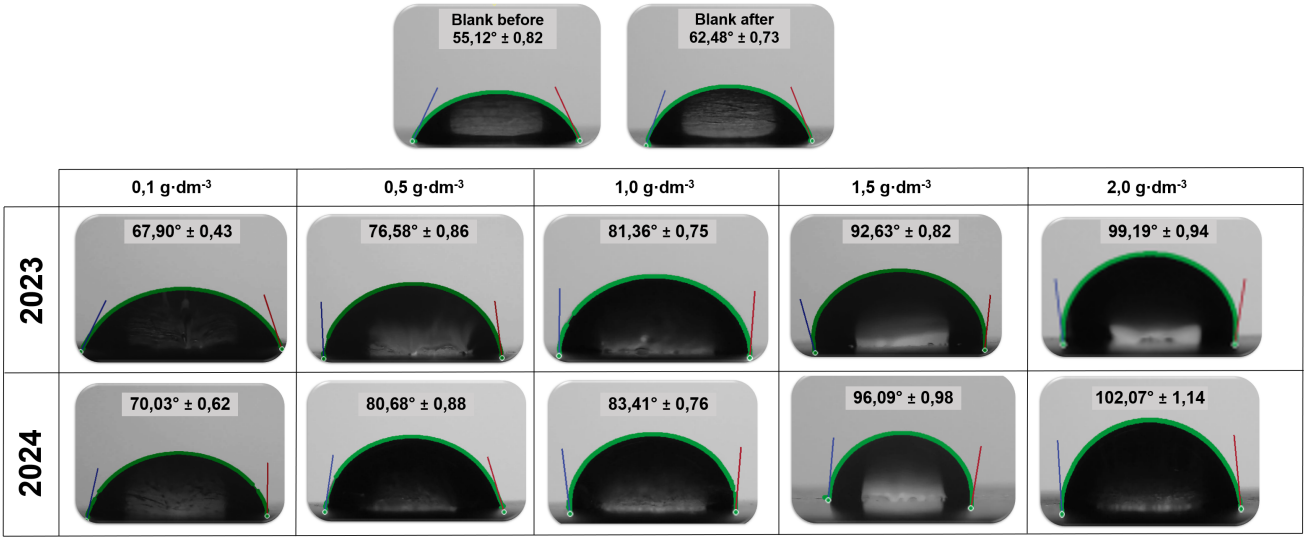

Figure 10. Contact angle values before and after immersing the D16T aluminum alloy in 0.1 mol·dm^{-3} NaOH solution for 8 hours in the absence and presence of different concentrations of *G. uralensis* leaves aqueous extract for 2023 and 2024.

Figure 10 shows that the contact angle on the polished surface of the D16T aluminum alloy is 55.12° ± 0.82 before immersion in a corrosive environment. After 24 hours of exposure to 0.1 mol·dm^{-3} NaOH without adding an inhibitor, the contact angle was determined to be 62.48°±0.73. In the presence of an inhibitor, the contact angle increases significantly with inhibitor concentration, reaching 102.07°±1.14 at the maximum concentration after 8 hours of immersion for the 2024 sample. The increase in contact angles with increasing inhibitor concentration indicates a corresponding increase in the metal surface's hydrophobicity. It reveals that the inhibitor is effectively adsorbed on the surface and forms a protective layer that reduces wettability. As the inhibitor concentration increases, this layer becomes stronger, further preventing the corrosion environment from interacting with the alloy surface.

The data obtained clearly confirm that the inhibitory effectiveness of the 2024 samples exceeds the same parameters for the 2023 samples. Obviously, these changes are due to a corresponding change in the phytochemical composition. The reason is most likely the spring flood of 2024, which inundated the area where the samples were collected. The self-regeneration of plants after floods involves increased photosynthesis to compensate for biomass loss (Mozo *et al.*, 2021). Since photosynthesis occurs in leaves, this leads to increased production of phenolic phytocomponents, which account for the increased inhibition efficiency.

Conclusion

This study shows that the aqueous extracts of *G. uralensis* leaves collected in 2023 and 2024 exhibit excellent inhibitory activity against the corrosion of D16T aluminum alloy in 0.1 mol·dm^{-3} NaOH solution. It was found that at a concentration of 2.0 g·dm^{-3}, the studied extracts exhibit inhibition efficiencies of up to 80.31% (2023) and 88.38% (2024) at 313K. The inhibitor spontaneously adsorbs on the metal surface, in accordance with the Langmuir, Freundlich, and Frumkin adsorption models, forming a protective film through physisorption. The developed inhibitor exhibits a mixed-type corrosion protection mechanism, predominantly hindering the cathodic reaction. It acts as an effective physical barrier, isolating the metal surface from the corrosive medium and thereby reducing the rates

of both electron transfer and diffusion processes involved in corrosion. Both the increase in temperature and the concentration of the inhibitor have a positive effect on the ability of the *G.uralensis* leaves aqueous extract to prevent corrosion, significantly enhancing the protective effect. The data of the electrochemical experiment and the results of the gravimetric measurements are in complete agreement. The increased protective effect of plant leaf extracts against corrosion after a flood may be attributed to the increased production of bioactive compounds, including phenols and flavonoids, in response to water stress. Flooding stimulates the production of these compounds, enhancing the protective properties of the extracts. These compounds form protective films on metal surfaces, reducing corrosion rates. Thus, the aqueous extract of *G. uralensis* leaves acts as an effective "green" inhibitor to prevent corrosion of D16T aluminum alloy in 0.1 mol·dm^{-3} NaOH solution. The findings of this study provide valuable insights for future investigations into the correlation between anticorrosive properties and plant growth conditions. They may also contribute to a better understanding of how both natural and anthropogenic environmental disturbances influence the development and effectiveness of corrosion inhibition systems.

Acknowledgement: The authors gratefully acknowledge the Head and staff of the Laboratory of Ecology and Biogeochemistry, M. Utemisov West Kazakhstan University, for providing the facilities, technical support, and assistance necessary to conduct this research.

Disclosure statement: *Conflict of Interest:* The authors declare that there are no conflicts of interest.
Compliance with Ethical Standards: This article does not contain any studies involving human or animal subjects.

References

Akatyev, N., & Samigolla, A. (2024). Sun protection properties and photostability of aqueous extracts of dandelion (*Taraxacum officinale* L.). *Prospects in Pharmaceutical Sciences*, 22(4), 160–167. https://doi.org/10.56782/pps.285

Akatyev, N., Kenzhegalieva, R., Khapiyeva, M., Uzakbay, G., Talapova, A., & Vardanyan, R. (2025). A new potential of sodium anthraquinone-2-sulfonate as a corrosion inhibitor for carbon steel in 0.5 M H_2SO_4. *Journal of Electrochemical Science and Engineering*, 2512. https://doi.org/10.5599/jese.2512

Al-Alimi, Yusuf N.K., Ghaleb A.M., Lajis G.A., *et al.* (2024). Recycling aluminium for sustainable development: A review of different processing technologies in green manufacturing, *Results in Engineering*, 23, 102566, https://doi.org/10.1016/j.rineng.2024.102566.

Al-Amiery A.A., Isahak W.N.R.W., Al-Azzawi W.K. (2023). Corrosion Inhibitors: Natural and Synthetic Organic Inhibitors. *Lubricants,* 11(4), 174. https://doi.org/10.3390/lubricants11040174

Aransiola, S. A., Josiah, I. U. J., Abioye, O. P., Bala, J. D., Rivadeneira-Mendoza, B. F., Prasad, R., Luque, R., Rodríguez-Díaz, J. M., & Maddela, N. R. (2024). Micro and vermicompost assisted remediation of heavy metal contaminated soils using phytoextractors. *Case Studies in Chemical and Environmental Engineering*, *9*, 100755. https://doi.org/10.1016/j.cscee.2024.100755

Arrousse, N., Salim, R., Houari, G. A., Hajjaji, F. E., ... & Quraishi, M. A. (2020). Experimental and theoretical insights on the adsorption and inhibition mechanism of (2E)-2-(acetylamino)-3-(4-nitrophenyl) prop-2-enoic acid and 4-nitrobenzaldehyde on mild steel corrosion. *Journal of Chemical Sciences*, 132(1), 112. https://doi.org/10.1007/s12039-020-01818-w

Bandeira, R.M., Lima, F.P., Nunes, M.S. *et al.* (2025). The green plant-based corrosion inhibitors—a sustainable strategy for corrosion protection. *Surf. Sci. Technol.* 3, 19, https://doi.org/10.1007/s44251-025-00084-7

Batah A, Al-Moubaraki AH, Noor EA, Al-Ahmari JM, Al-Ghamdi AA, Id El Mouden O, Salghi R, Chafiq M, Chaouiki A, Ko YG. Environmentally Benign Grape Seed Oil for Corrosion Inhibition: Cutting-Edge Computational Modeling Techniques Revealing the Intermolecular and Intramolecular Synergistic Inhibition Action. *Coatings*. 2024; 14(1):77. https://doi.org/10.3390/coatings14010077

Bazzi I., Hamdani I., Kadda S., Zaidi K., Merimi C., Loukili E. (2023). Corrosion inhibitors of mild steel in acidic solution: A bibliometric analysis from 1990 to 2023, *Afr. J. Manag. Engg. Technol.* 1 (1), 76-89

Eddy, & Ebenso. (2008). Adsorption and inhibitive properties of ethanol extracts of Musa sapientum peels as a green corrosion inhibitor for mild steel in H_2SO_4. *African Journal of Pure and Applied Chemistry*, *2*(6), 046–054. https://doi.org/10.5897/ajpac.9000008

El-Azabawy, O. E., Higazy, S. A., Al-Sabagh, A. M., Abdel-Rahman, A. A., Nasser, N. M., & Khamis, E. A. (2022). Studying the temperature influence on carbon steel in sour petroleum media using facilely-designed Schiff base polymers as corrosion inhibitors. *Journal of Molecular Structure*, *1275*, 134518. https://doi.org/10.1016/j.molstruc.2022.134518

El Azzouzi, M. Azzaoui, K., Warad, I., ... Lamhamdi, A., Zarrouk, A. (2022). Moroccan, Mauritania, and senegalese gum Arabic variants as green corrosion inhibitors for mild steel in HCl: Weight loss, electrochemical, AFM and XPS studies, *Journal of Molecular Liquids*, 347, 118354, https://doi.org/10.1016/j.molliq.2021.118354

El-Etre, A. (1998). Natural honey as corrosion inhibitor for metals and alloys. i. copper in neutral aqueous solution. *Corrosion Science*, *40*(11), 1845–1850. https://doi.org/10.1016/s0010-938x(98)00082-1

El-Etre, A., Abdallah, M., El-Tantawy, Z. (2004). Corrosion inhibition of some metals using lawsonia extract. *Corrosion Science*, *47*(2), 385–395. https://doi.org/10.1016/j.corsci.2004.06.006

Ettahiri, W., Al Ati, G., Salim, R., Chkirate, K., Hammouti, B., Achour, R., ... & Taleb, M. (2024). Synthesis and characterization of pyrazole-acetamide schiff bases as highly effective inhibitors for mild steel in 1 M HCl. *Journal of Industrial and Engineering Chemistry*, 140, 545-555. https://doi.org/10.1016/j.jiec.2024.06.013

Fouda, A. S., Megahed, H. E., Fouad, N., & Elbahrawi, N. M. (2016). Corrosion Inhibition of Carbon Steel in 1 M Hydrochloric Acid Solution by Aqueous Extract of Thevetia peruviana. *Journal of Bio- and Tribo-Corrosion*, *2*(3). https://doi.org/10.1007/s40735-016-0046-z

Ghazoui, A., Zarrouk, A., Bencaht, N., Salghi, R., Assouag, M., El Hezzat, M., ... & Hammouti, B. (2014). New possibility of mild steel corrosion inhibition by organic heterocyclic compound. *J. Chem. Pharm. Res*, 6(2), 704-712.

Hajjaji, F. E., Belghiti, M. E., Drissi, M., Fahim, M., Salim, R., ... & Nahle, A. (2019). Electrochemical, quantum calculations and monte carlo simulation studies of N1, N2-Bis (1-phenylethylidene) ethane-1, 2-diamine as a corrosion inhibitor for carbon steel in a 1.0 M hydrochloric acid solution. *Portugaliae Electrochimica Acta*, 37(1), 23-42.

Hmamou B.D., Salghi R., Zarrouk A., Messali M., Zarrok H., Errami M., Hammouti B., Bazzi Lh., Chakir A. (2012) Inhibition of steel corrosion in hydrochloric acid solution by chamomile extract, *Der Pharma Chim*. 4 N°4, 1496-1505.

ISO (2021). 8407: 2021; Corrosion of Metals and Alloys—Removal of Corrosion Products from Corrosion Test Specimens. *International Organization for Standardization (ISO): Geneva, Switzerland*.

Khadraoui A., Khelifa A., Boutoumi H., *et al*. (2014). Corrosion inhibition of carbon steel in hydrochloric acid solution by Mentha pulegium extract, A *Portugaliae Electrochimica Acta,* 32 (4), 271-280

Langelandsvik, G., Akselsen, O. M., Furu, T., & Roven, H. J. (2021). Review of Aluminum Alloy Development for Wire Arc Additive Manufacturing. *Materials*, *14*(18), 5370. https://doi.org/10.3390/ma14185370

Li, B., Wang, W., Chen, L., Zheng, X., Gong, M., Fan, J., Tang, L., Shi, Q., & Zhu, G. (2023). Corrosion inhibition effect of magnolia grandiflora leaves extract on mild steel in acid solution. *International Journal of Electrochemical Science*, *18*(4), 100082. https://doi.org/10.1016/j.ijoes.2023.100082

Liu, Q., Zheng, T., Wang, P., Jiang, J., & Li, N. (2009). Adsorption isotherm, kinetic and mechanism studies of some substituted phenols on activated carbon fibers. *Chemical Engineering Journal*, *157*(2–3), 348–356. https://doi.org/10.1016/j.cej.2009.11.013

Loto, R. T. (2022). Investigation of the protection effect of ginger, tea tree and grapefruit essential oil extracts on mild steel in 0.5M H_2SO_4 solution. *Materials Research Express*, *9*(6), 066509. https://doi.org/10.1088/2053-1591/ac7852

Loukili E.H., Kadda S., Azzaoui K., Bouklah M. (2023). Adsorption of organic inhibitors on metal surface: isotherm models, *EHEI-Journal of Science & Technology*, 3 (2), 95–107

Lrhoul H., Sekkal H., Hammouti B. (2023) Natural Plants as Corrosion Inhibitors: Thermodynamic's restrictions, *Mor. J. Chem.,*14(3), 689-698, https://doi.org/10.48317/IMIST.PRSM/morjchem-v11i3.40144

Miralrio, A., & Vázquez, A. E. (2020). Plant extracts as green corrosion inhibitors for different metal surfaces and corrosive media: a review. *Processes*, *8*(8), 942. https://doi.org/10.3390/pr8080942

Mozo, I., Rodríguez, M. E., Monteoliva, S., & Luquez, V. M. (2021). Floodwater depth causes different physiological responses during post-flooding in willows. *Frontiers in Plant Science*, 12, 575090. https://doi.org/10.3389/fpls.2021.575090

Nailya, S., Zhanat, S., Raushan, T., & Asker, T. (2018). Polyphenolic compounds of plant of Lepidium Ruderale Linn. and their biological activity. *Journal of Biochemical Technology*, *9*(4-2018), 77-80.

Nwabanne, J. T., & Okafor, V. N. (2012). Adsorption and thermodynamics study of the inhibition of corrosion of mild steel in H_2SO_4 medium using Vernonia amygdalina. *Journal of Minerals and Materials Characterization and engineering*, *11*(09), 885.

Ostovari, A., Hoseinieh, S., Peikari, M., Shadizadeh, S., & Hashemi, S. (2009). Corrosion inhibition of mild steel in 1M HCl solution by henna extract: A comparative study of the inhibition by henna and its constituents (Lawsone, Gallic acid, α-d-Glucose and Tannic acid). *Corrosion Science*, *51*(9), 1935–1949. https://doi.org/10.1016/j.corsci.2009.05.024

Paz Martínez-Viademonte M., Abrahami S.T., Hack T., Burchardt M., Terryn H. (2020). A Review on Anodizing of Aerospace Aluminum Alloys for Corrosion Protection. *Coatings.* 10(11), 1106. https://doi.org/10.3390/coatings10111106

Peng, T., Ren, L., Du, E., Ou, X., & Yan, X. (2022). Life cycle energy consumption and greenhouse gas emissions analysis of primary and recycled aluminum in China. *Processes*, *10*(11), 2299. https://doi.org/10.3390/pr10112299

Raja, P. B., & Sethuraman, M. G. (2007). Natural products as corrosion inhibitor for metals in corrosive media — A review. *Materials Letters*, *62*(1), 113–116. https://doi.org/10.1016/j.matlet.2007.04.079

Salim, R., Adardour, M., Ettahiri, W., Ech-chihbi, E., Hammouti, B., Azam, M., ... & Taleb, M. (2024). Computational and electrochemistry of effective triazolyl-benzimidazolone inhibitors in aggressive environment. *Sustainable Materials and Technologies*, 39, e00862. https://doi.org/10.1016/j.susmat.2024.e00862

Seilova, T., Runasheva, Z., Kubasheva, R., & Akatyev, N. (2024). Development of new three-component BNP-inhibitor for carbon steel in 0.5 mol·dm^{-3} HCl solution. Thermodynamic, adsorption and electrochemical studies. *International Journal of Corrosion and Scale Inhibition*, *13*(2). https://doi.org/10.17675/2305-6894-2024-13-2-33

Solmaz, R., Kardaş, G., Yazıcı, B., & Erbil, M. (2007). Adsorption and corrosion inhibitive properties of 2-amino-5-mercapto-1,3,4-thiadiazole on mild steel in hydrochloric acid media. *Colloids and Surfaces a Physicochemical and Engineering Aspects*, *312*(1), 7–17. https://doi.org/10.1016/j.colsurfa.2007.06.035

Tsygankova, L. E., Vigdorovich, V. I., Shel, N. V., & Dubinskaya, E. V. (2013). Peculiarities of protective efficiency of nitrogen containing inhibitors of steel corrosion. *International Journal of Corrosion and Scale Inhibition*, *2*(4), 304-310.

Umoren, S. A., Ebenso, E. E., Okafor, P. C., Ekpe, U. J., & Ogbobe, O. (2006). Effect of halide ions on the corrosion inhibition of aluminium in alkaline medium using polyvinyl alcohol. *Journal of Applied Polymer Science*, *103*(5), 2810–2816. https://doi.org/10.1002/app.25446

Valiev, A. M., Kharisov, L. R., Pankratov, D. L., & Gatin, R. N. (2020). Development of manganese master alloy for aluminum alloys and the technology of its application. *Int. J. Eng. Res. Technol*, *13*(11), 3736-3740.

Wang L., Zhang K., Han S., Zhang L., Bai H., Bao F., *et al.* (2019). Constituents Isolated from the Leaves of Glycyrrhiza uralansis and Their Anti-Inflammatory Activities on LPS-Induced RAW264.7 Cells. *Molecules.* 24(10), 1923. https://doi.org/10.3390/molecules24101923